Radiosynthesis and biological evaluation of the new PDE10A radioligand [^{18}F]AQ28A

Wagner, S.; Teodoro, R.; Deuther-Conrad, W.; Kranz, M.; Scheunemann, M.; Fischer, S.; Wenzel, B.; Egerland, U.; Hoefgen, N.; Steinbach, J.; Brust, P.;

Originally published:

November 2016

Journal of Labelled Compounds and Radiopharmaceuticals 60(2017)1, 36-48

DOI: https://doi.org/10.1002/jlcr.3471

Radiosynthesis and biological evaluation of the new PDE10A radioligand AQ28A

Sally Wagner[a], Rodrigo Teodoro[a,*], Winnie Deuther-Conrad[a], Mathias Kranz[a], Matthias Scheunemann[a], Steffen Fischer[a], Barbara Wenzel[a], Ute Egerland[b], Norbert Hoefgen[b], Jörg Steinbach[a] and Peter Brust[a]

[a]*Helmholtz-Zentrum Dresden-Rossendorf, Institute of Radiopharmaceutical Cancer Research, Research Site Leipzig, Dept. of Neuroradiopharmaceuticals, Permoserstraße 15, 04318 Leipzig*, Germany
[b]*BioCrea GmbH, Meißner Straße 191, 01445 Radebeul, Germany*

Cyclic nucleotide phosphodiesterase 10A (PDE10A) regulates the level of the second messengers cAMP and cGMP in particular in brain regions assumed to be associated with neurodegenerative and psychiatric diseases. A better understanding of the pathophysiological role of the expression of PDE10A could be obtained by quantitative imaging of the enzyme by positron emission tomography (PET). Thus, in this study we developed, radiolabeled and evaluated a new PDE10A radioligand, 8-bromo-1-(6-[^{18}F]fluoropyridin-3-yl)-3,4-dimethylimidazo[1,5-*a*]quinoxaline ([^{18}F]**AQ28A**). [^{18}F]**AQ28A** was radiolabeled by both nucleophilic bromo-to-fluoro or nitro-to-fluoro exchange using K[^{18}F]F-$K_{2.2.2}$-carbonate complex with different yields. Using the superior nitro precursor, we developed an automated synthesis on a Tracerlab™ FX F-N module and obtained [^{18}F]**AQ28A** with high radiochemical yields (33±6%) and specific activities (96-145 GBq/µmol) for further evaluation. Initially, we investigated the binding of [^{18}F]**AQ28A** to the brain of different species by autoradiography and observed the highest density of binding sites in striatum, the brain region with the highest PDE10A expression. Subsequent dynamic PET studies in mice revealed a region-specific accumulation of [^{18}F]**AQ28A** in this region, which could be blocked by pre-injection of the selective PDE10A ligand MP-10. In conclusion, the data suggest [^{18}F]**AQ28A** is a suitable candidate for imaging of PDE10A in rodent brain by PET.

Keywords: PDE10 radioligand, ^{18}F-labeled radioligand, automated synthesis, nitro precursor, bromo precursor, Animal PET/MR

Introduction

Cyclic nucleotide phosphodiesterases (PDEs) are a superfamily of enzymes which are integral constituents of the second messenger signaling cascade,[1] that hydrolyze and thus inactivate the cyclic nucleotides cAMP and cGMP. Until now 11 families of PDEs are known which are encoded by 21 genes. One of these families, phosphodiesterase 10A (PDE10A), has been characterized as a dual substrate enzyme with unique expression pattern and kinetic properties.[2] PDE10A is abundantly expressed in brain, in particular in the medium spiny neurons of the striatum.[2-5] The striatum is the largest component of the basal ganglia, a system of interconnected nuclei which regulates psychomotor behavior.[6] According to this, the striatum receives and processes information from the cortex and thalamus and projects to the globus pallidus and substantia nigra, pars reticulata.[7] The striatal neuron population consists mainly

(90%) of medium spiny neurons (MSN). MSNs receive excitatory, glutaminergic inputs from cortex and thalamus and dopaminergic innervation from substantia nigra, serving to modulate the glutamatergic stimulation. They are divided in two classes of neurons, those expressing D_1 receptors and projecting to the substantia nigra pars reticulata (striatonigral direct pathway), and those expressing D_2 receptors and projecting to the globus pallidus (striatopallidal indirect pathway).[8] $D_{1/2}$ receptors are G-protein coupled receptors (GPCRs),[9] which activate (D_1) or inhibit (D_2) intracellular signalling via cAMP-dependent protein kinase A (PKA). PDE10A is associated with the post-synaptic membranes of MSNs and modulates MSN excitability by the breakdown of cAMP and cGMP.[10] Thus, inhibition of PDE10A has effects similar to those of D_2 antagonists and D_1 agonists regarding cyclic nucleotide levels.[11-13] In contrast to selective D_2 antagonists and D_1 agonists, PDE10A inhibitors activate both pathways equally and thereby provide a unique potential to treat diseases linked to striatal dysfunction such as schizophrenia,[14, 15] Huntington's disease[16, 17] or obsessive compulsive disorder. Significant understanding of the biological role of PDE10A as achievable by positron emission tomography (PET) would support the development of new therapeutic strategies. Besides measuring the enzyme levels under (patho)physiological conditions, a suitable PDE10A radioligand could be used to determine PDE10A occupancy of drugs. Up to now several PDE10A radioligands have been developed,[18-21] the majority labeled with ^{11}C, e.g. [^{11}C]MP10, [^{11}C]IMA107 or [^{11}C]LuAE92686,[22-24] and a few ^{18}F-labeled (Figure 1) such as [^{18}F]JNJ41510417 and the more suitable [^{18}F]JNJ42259152,[25, 26] already tested in humans.[27, 28] Furthermore, the 2-(2-(3-aryl-4-oxo-3,4-dihydroquinazolin-2-yl)ethyl)isoindoline-1,3-diones [^{18}F]MNI654 and [^{18}F]MNI659 have been identified as potential PDE10A radioligands[29, 30] with [^{18}F]MNI659 investigated in humans,[20, 30-32] and recently the 1-(4-(3-(4-(1H-benzo[d]imidazole-2-carbonyl)phenoxy)pyrazin-2-yl)piperidin-1-yl)-2-fluoropropan-1-one [^{18}F]AMG580 was developed and tested in non-human primates.[33, 34]

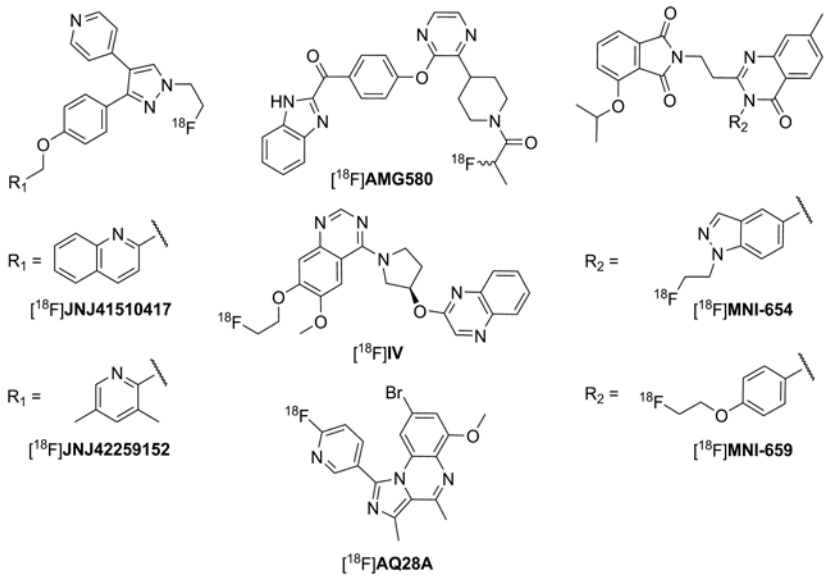

Figure 1. Reported ^{18}F-labeled PDE10A radioligands.

We obtained a ^{18}F-labeled ligand from a series of (*R*)-6,7-dimethoxy-4-(3-(quinoxalin-2-yloxy)pyrrolidin-1-yl)quinazoline (PQ-10) derivatives,[35] however, [^{18}F]**IV** (Figure 1) proved to be nonselective in vivo.[36] 1-arylimidazo[1,5-*a*]quinoxalines were reported as a new class of compounds characterized by high inhibitory potency and selectivity for PDE10A as well as pronounced *in vitro* stability.[37] Based on this hit, very recently we reported on the synthesis of 16 new fluorinated arylimidazo[1,5-*a*]quinoxalines by introducing fluorine at an aromatic position to increase the metabolic stability of potential PET radioligands and evaluated their inhibitory potential (IC_{50}=2.95 nM) and selectivity towards PDE10A (IC_{50} for all other PDEs >1000 nM).[38,39] From this series of PDE10A inhibitors, we identified **AQ28A** as most suitable for the development of a corresponding radioligand. Herein we report on the development and evaluation of [^{18}F]**AQ28A** (Scheme 1) including precursor synthesis, ^{18}F-radiolabeling optimization and transfer to a fully automated setup. In addition, we conducted i) *in vitro* autoradiography studies on mouse, rat and pig brain slices, ii) e*x vivo* studies to inspect for radiometabolites in plasma and brain and iii) *in vivo* PET evaluation assessing pharmacokinetics and target selectivity of [^{18}F]**AQ28A** in mice under baseline and blocking conditions.

Experimental section

General method

Chemicals were purchased in high quality from Aldrich, Acros, Apollo scientific, Fluka and Merck and used without further purification. Air and moisture sensitive reactions were carried out under

a stream of argon. 1,4-Dioxane was dried over sodium/benzophenone and distilled. Flash chromatography was performed on silica gel 60 (0.04-0.063 mm) from Merck. NMR spectra were recorded on Varian Mercury 300BB (300 MHz for ^{1}H, 75 MHz for ^{13}C, 282 MHz for ^{19}F) or Varian Mercury 400BB (400 MHz for ^{1}H, 101 MHz for ^{13}C). Chemical shifts δ are reported in ppm and referred to the solvent ($CHCl_3$: 7.26, $CDCl_3$: 77.16) as internal standard. Multiplicities of signals are indicated as follows: singlet (s), doublet (d), triplet (t), broad signal (br). Mass spectra were recorded on a ESQUIRE 3000 Plus (ESI, low resolution) and a 7 Tesla APEX II (ESI, high resolution) from Bruker Daltonics.

Pre-coated thin layer chromatography (TLC) Polygram® SIL G/UV_{254} plates obtained from Macherey-Nagel were used for thin layer chromatography. Spots were detected by UV irradiation (λ = 254 nm). Radio-TLC was performed on Polygram® SIL G/254 nm plates (Macherey-Nagel GmbH & Co. KG, Düren, Germany) with THF/cyclohexane 8/3 (v/v; R_f=0.5), analyzed using a BAS-1800 II system Bioimaging Analyzer (Fuji Photo Film, Co. Ltd., Tokyo, Japan) and evaluated with AIDA 2.31 software (raytest Isotopenmessgeräte GmbH, Straubenhardt, Germany).

No carrier added (n.c.a.) [^{18}F]fluoride ($t_{1/2}$ = 109.8 min) was produced by irradiation of a [^{18}O]water target on a Cyclone®18/9 (iba RadioPharma Solutions, Louvain-la-Neuve, Belgium) via the $^{18}O(p,n)^{18}F$ nuclear reaction. For radioactivity measurements an ISOMED2010 (MED GmbH, Dresden, Germany) dose calibrator was used. Solid phase extraction (SPE) was carried out on Sep Pak® C18 Plus light cartridges (Waters, Milford, MA, USA; pre-conditioned with 5 mL of absolute EtOH or MeOH and 50 mL water). Semi-preparative and analytical HPLC was performed on JASCO system at λ=254 nm equipped with a radioactivity-HPLC flow monitor (Gabi Star, raytest GmbH, Straubenhardt, Germany).

For semi-preparative HPLC system **A** (precolumn + column: Multospher 120 RP 18-AQ, 50×10 mm + 150 × 10 mm, particle size 5 µm; (CS-Chromatographie Service GmbH, Germany); eluent (isocratic): MeCN/NH_4HCO_2 aq. (20 mM) 40/60 (v/v), 3 mL/min) and system **B** (Precolumn + column: Reprosil-Pur C18-AQ, 50 × 10 mm + 150 × 10 mm, particle size 10 µm (Dr. Maisch GmbH, Germany); eluent (isocratic): MeCN/H_2O/TFA 30/70/0.05 (v/v/v), 3 mL/min) were used.

For analytical HPLC system **C** (column: Reprosil-Pur C18-AQ, 250 × 4.0 mm, particle size 5 µm (Dr. Maisch GmbH, Germany); eluent (gradient): 10% MeCN (0→10 min), 10-80% MeCN (10→40 min), 80% MeCN (40→50 min) in 20 mM NH_4OAc aq., 1 mL/min), and system **D** (column: Reprosil-Pur C18-AQ, 250 × 4.0 mm, particle size 5 µm; eluent (isocratic): MeCN/NH_4OAc aq. (20 mM) 36/74 (v/v), 1 mL/min) were used.

Specific activity was determined based on a calibration curve obtained under isocratic HPLC conditions (system **D)** using chromatograms acquired at 240 nm, an appropriate maximum UV

absorbance of the corresponding reference compound **AQ28A** (8-bromo-6-methoxy-3,4-dimethyl-1-(6-fluoropyridin-3-yl)imidazo[1,5-a]quinoxaline).[38]

Remote controlled automated synthesis was performed using a TRACERlab™ FX F-N synthesizer (GE Healthcare, Waukesha, WI, USA) equipped with a PU-980 pump (JASCO, Gross-Umstadt, Germany), a WellChrom K-2001 UV detector (KNAUER GmbH, Berlin, Germany), NaI(Tl)-counter and automated data acquisition (NINA software version 4.8 rev. 4, Nuclear Interface GmbH, Dortmund, Germany).

Synthesis of precursors

*8-Bromo-1-(6-bromopyridin-3-yl)-6-methoxy-3,4-dimethylimidazo[1,5-a]quinoxaline (**AQ46**)*

Argon was bubbled for 15 min through a suspension of compound **1** (300 mg, 0.8 mmol) (Scheme 1) and K_2CO_3 (161 mg, 1.2 mmol) in a 1,4-dioxane-water mixture (4/1, v/v) (15 mL). 2-Bromopyridin-5-boronic acid **2** (236 mg, 1.2 mmol) and $Pd(PPh_3)_4$ (90 mg, 0.08 mmol) were added and the mixture was refluxed for 23 h. After cooling the reaction mixture to ambient temperature, water (15 mL) was added and a solid precipitated. The solid was filtered off and the filtrate was extracted with CH_2Cl_2 (3 × 7 mL). The combined organics were separated by flash chromatography [CH_2Cl_2/ethyl acetate 5/1 (v/v)]. Fractions containing the product were pooled and evaporated followed by precipitation from chloroform/petroleum ether. AQ46 was obtained as a colorless solid in 15% yield (56 mg). 27% of starting material was recovered. M.p. 322-334 °C (dec.); **^{1}H NMR** (300 MHz, $CDCl_3$): δ = 8.69 (dd, *J* = 2.5, *J* = 0.6 Hz, 1H), 7.83 (dd, *J* = 8.2 Hz, *J* = 2.5 Hz, 1H), 7.69 (dd, *J* = 8.2 Hz, *J* = 0.6 Hz, 1H), 7.12 (d, *J* = 1.8 Hz, 1H), 7.04 (d, *J* = 1.8 Hz, 1H), 4.04 (s, 3H), 2.89 (s, 3H), 2.80 (s, 3H). **^{13}C NMR** (101 MHz, $CDCl_3$): δ = 156.3, 153.7, 150.6, 143.8, 139.1, 137.7, 137.5, 128.2, 127.6, 127.4, 126.8, 123.5, 120.4, 112.0, 111.5, 57.0, 24.7, 16.3. **HRMS (ESI+):** *m/z* = 460.9607 (calc. 460.9607 for $C_{18}H_{15}{}^{79}Br_2N_4O$ $[M+H]^+$).

*2-Nitro-5-(4,4,5,5-tetramethyl-1,3,2-dioxaborolan-2-yl)pyridine (**3**)*

In a two-necked flask 5-bromo-2-nitropyridine (1.50 g, 7.4 mmol) and potassium acetate (3.62 g, 36.9 mmol) were suspended in 30 mL of freshly dried 1,4-dioxane. After degassing the mixture, bis(pinacolato)diborane (1.88 g, 7.4 mmol) and $PdCl_2$(dppf) (216 mg, 0.29 mmol) were added and the mixture was refluxed for 90 min. The reaction mixture was cooled to ambient temperature and filtered through a plug of celite. The solvent was removed and the residue purified by column chromatography using a short column packed with silica (petroleum ether/ethyl acetate 1/1 (v/v). After concentration of the collected fractions, compound **3** was crystallized successively, isolated and washed with *n*-hexane to give a colorless solid (1.36 g, 74%). M.p. 144-145 °C; **^{1}H NMR** (400 MHz, $CDCl_3$): δ = 8.93 (s, 1H), 8.39 (d, *J* = 8.0 Hz, 1H),

8.21 (d, *J* = 8.0 Hz, 1H), 1.37 (s, 12H). **^{13}C NMR** (101 MHz, $CDCl_3$) δ = 158.33, 154.80, 146.45, 117.00, 85.22, 24.98, C-NO_2 was not detected. **LRMS (ESI+):** *m/z* = 251.2 (calc. 251.1 for $C_{11}H_{16}BN_2O_4$ $[M+H]^+$).

*8-Bromo-6-methoxy-3,4-dimethyl-1-(6-nitropyridin-3-yl)imidazo[1,5-a]quinoxaline (**AQ63**)*

Compound **1** (230 mg, 0.6 mmol), **3** (195 mg, 0.8 mmol) and K_2CO_3 (249 mg, 1.8 mmol) were suspended in a 1,4-dioxane-water mixture (4/1, v/v) (13 mL) and flushed with argon for 15 min. After adding $Pd(PPh_3)_4$ (34 mg, 0.03 mmol), the mixture was refluxed for 12 h. Additional portions of **3** (55 mg, 0.2 mmol) and $Pd(PPh_3)_4$ (17 mg, 0.015 mmol) were added and the mixture was refluxed for further 6 h. After cooling, the solvent was removed and the residue was portioned between chloroform (50 mL) and water (20 mL). The aqueous layer was separated and extracted again with $CHCl_3$ (2 × 15 mL). Combined organic layers were washed with brine, dried over $MgSO_4$ and the solvent was removed under reduced pressure. Column chromatography on silica using CH_2Cl_2/ethyl acetate 5/1 (v/v) as eluent followed by precipitation from a $CHCl_3$-petroleum ether mixture yielded 73 mg (28%) of **AQ63** as a yellow solid. 30% of starting material was recovered. M.p. 338-346 °C (dec.); **^{1}H NMR** (400 MHz, $CDCl_3$): δ = 9.01 (d, *J* = 1.9 Hz, 1H), 8.48 (d, *J* = 8.4 Hz, 1H), 8.38 (dd, *J* = 8.4 Hz, *J* = 2.2 Hz, 1H), 7.11 (d, *J* = 1.6 Hz, 1H), 7.09 (d, *J* = 1.7 Hz, 1H), 4.09 (s, 3H), 2.92 (s, 3H), 2.83 (s, 3H). Due to the low solubility of the product in several solvents no ^{13}C NMR was obtained. **HRMS (ESI+):** *m/z* = 428.0351 (calc. 428.0353 for $C_{18}H_{15}{}^{79}BrN_5O_3$ $[M+H]^+$)

Radiochemistry

General procedure for manual radiosynthesis optimization

Aqueous n.c.a. [^{18}F]fluoride was trapped on a Chromafix® 30 PS-HCO_3^- cartridge (Macherey-Nagel GmbH & Co. KG, Düren, Germany) and eluted with 300 µL of an aqueous K_2CO_3 solution (1.78 mg, 12.9 µmol). Thereafter, Kryptofix®2.2.2. ($K_{2.2.2.}$, 11.2 mg, 29.7 µmol) in 1 mL of MeCN was directly transferred to the reaction vial and the mixture was azeotropically dried under vacuum. The final complex was dissolved in 500 µL solvent for radiolabeling. Labeling conditions were optimized regarding the solvent [MeCN, *N,N*-dimethylformamide (DMF) and dimethyl sulfoxide (DMSO)], reaction temperature (120°, 140°C) time (up to 20 min) and heating mode [conventional or microwave-assisted heating (Discover PETwave Microwave CEM®)] using a constant concentration (50%) of the K[^{18}F]F-$K_{2.2.2}$-carbonate complex for each reaction. Aliquots of the reaction mixture were analyzed by radio-TLC after 5, 10, 15 and 20 min.

Radiosynthesis of [^{18}F]AQ28A starting from AQ46

K[^{18}F]F-$K_{2.2.2}$-carbonate complex was prepared and dissolved in 500 µL anhydrous DMSO. The reaction took place with a mixture of the bromo precursor **AQ46** (1 mg in 250 µL DMSO) and 250 µL of complex solution (50%) at 140°C for 10 min. After cooling, the reaction mixture was diluted with 2.5 mL MeCN/H_2O 1/1 (v/v) and injected onto a semi-preparative radio-HPLC (system **A**, t_R = 20.2 min). The fractions containing [^{18}F]**AQ28A** were collected and diluted with water to a total volume of 50 mL. Thereafter, the solution was passed through a Sep Pak® C18 Plus cartridge, washed with 2 mL H_2O and [^{18}F]**AQ28A** was subsequently eluted with 1500 µL ethanol. The solvent was reduced under a stream of nitrogen at 70°C (approximately 50 µL), and [^{18}F]**AQ28A** was formulated with the addition of sterile isotonic saline solution up to a final concentration of 10% EtOH (v/v). Analytical characterization of [^{18}F]**AQ28A** was performed by radio-HPLC (system **C**) and radio-TLC (see General method). The identity of the product was confirmed by co-injection of the corresponding reference compound **AQ28A** (system **C**).

Automated radiosynthesis of [^{18}F]AQ28A starting from AQ63

Optimal radiolabeling conditions were further translated to an automated setup using a TRACERlab™ FX F-N synthesizer. K[^{18}F]F-$K_{2.2.2}$-carbonate complex was obtained after trapping [^{18}F]F^- (2-15 GBq) on a Chromafix® 30 PS-HCO_3^- cartridge, subsequent elution with a K_2CO_3 solution (1.78 mg/0.4 mL water), and followed by the addition of $K_{2.2.2}$ (11.5 mg/1 mL MeCN). The nucleophilic aromatic radiofluorination proceeded using the nitro precursor **AQ63** (1 mg/0.75 mL DMSO) at 120°C for 8 min. The reaction mixture was cooled and diluted with 3 mL of MeCN/H_2O 1/1 (v/v). Thereafter, [^{18}F]**AQ28A** was isolated by semi-preparative HPLC (system **B**, t_R = 28.0 min). Final purification step took place after passing the solution with a Sep Pak® C18 Plus cartridge, followed by washing with 2 mL of water and elution of [^{18}F]**AQ28A** with 1.5 mL of ethanol. The solvent was reduced under a stream of nitrogen at 70°C and the desired radiotracer was formulated as an injectable solution in isotonic saline containing 10% ethanol (~1 MBq/µL final concentration). Analytical characterization of [^{18}F]**AQ28A** was performed by radio-HPLC (system **C** and system **D**) and radio-TLC. The identity of the product was confirmed by co-injection of the corresponding reference compound **AQ28A** (system C). Labeling efficiencies for the automated process were calculated based on TLC analysis after the syntheses using samples from remaining solution in the injection vial.

Chemical stability and logD determination

The chemical stability of [^{18}F]**AQ28A** was analyzed in formulation for 3 hours and in phosphate buffered saline (PBS, pH 7.4) and TRIS-HCl (pH 7.2) for one hour (~ 2-3 MBq in 200 µL buffer).

Aliquots were taken each hour and analyzed by radio-TLC. Likewise, the stability of [^{18}F]**AQ28A** was investigated for 1 hour at 37°C in pig plasma (9 MBq in 500 µL medium).

The lipophilicity of [^{18}F]**AQ28A** was estimated by the conventional shake-flask method. For each buffer system (PBS, pH 7.4, or TRIS-HCl, pH 7.2), 8 µL of the formulated radiotracer (~1.6 MBq) was added to 3 mL of buffer and mixed with 3 mL *n*-octanol. The tubes were shaken for 20 min using a mechanical shaker (HS250 basic, IKA Labortechnik GmbH & Co. KG, Staufen, Germany) followed by centrifugation (5500 rpm for 5 min). After phase separation, aliquots (1 mL) were taken from the organic and the aqueous phase and the radioactivity was measured using a gamma counter (1480 WIZARD, Fa. Perkin Elmer, Waltham, MA, USA). A volume of 1 mL of the organic phase was taken, added to a volume of 6 mL buffer/*n*-octanol 1/1 (v/v) and treated as previously described. The distribution coefficient (*D*) was calculated as [radioactivity (cpm/mL) in *n*-octanol]/[radioactivity (cpm/mL) in buffer] and reported as the decade logarithmic value (log*D*).

In vitro and *in vivo* characterization

All animal experiments were approved (TVV08/13, Landesdirektion Sachsen, Freistaat Sachsen, Germany) and performed according to the local rules and regulations.

Determination of *in vitro* affinity

The *in vitro* affinity (K_D) of [^{18}F]**AQ28A** for rat PDE10A has been determined from a homologous binding experiment. Membrane homogenates were prepared from rat striatum, isolated from female SPRD rats (10-12 weeks), and incubated with 0.18 MBq/mL [^{18}F]**AQ28A** (specific activity = 57 GBq/µmol; chemical concentration = 3.16 nM) and seven concentrations of **AQ28A** in the range of 10^{-11} M to 10^{-5} M in binding buffer (50 mM TRIS-HCl (pH 7.4), 120 mM NaCl, 5 mM KCl, and 1 mM $MgCl_2$) at room temperature for 60 min. The incubation was terminated by rapid filtration in a 48-sample harvester (Brandel, Gaithersburg, MD, USA) via GF/B glass-fibre filter (Whatman, GE Healthcare Bio-Sciences, Pittsburgh, PA, USA) presoaked for 60 min in 0.3% polyethylenimine. The radioactivity bound at the filter was measured using a gamma counter. The obtained homologous competitive binding curve was evaluated by nonlinear regression (GraphPad Prism 6, GraphPad Software, Inc., La Jolla, CA, USA) and the K_D was calculated according to the conversion of the Cheng and Prusoff equation: $K_i = K_D = IC_{50} - [\text{Radioligand}]$.[40]

In vitro autoradiography

Brains were obtained from juvenile female German landrace pigs (10-13 kg initially sedated with ketamine hydrochloride (20 mg/kg) and midazolam (1 mg/kg), maintained during i.v. catheter

application (jugular vein) by 70% NO in 30% O_2 and 2 Vol-% isoflurane; animals were sacrificed by bolus injection of 10 ml saturated KCl solution), and female young adult SPRD rats (10-12 weeks; decapitation after CO_2 inhalation) and CD1 mice (10-12 weeks; manual cervical dislocation). The respective tissues were frozen in isopentane at -30°C directly after isolation, and cryosectioned using a cryomicrotome (Microm HM 560; Thermo Fisher Scientific Inc., Walldorf, Germany). The cryosections (mouse and rat = 12 µm; pig = 20 µm) were transferred to microscope slides, dried at room temperature, and stored at -25°C until use. For autoradiographic experiments, the sections were thawed and dried at room temperature, and incubated for 60 min in TRIS buffer (50 mM; pH 7.4/21°C) containing 120 mM NaCl, 5 mM KCl, 2 mM $CaCl_2$, and 2 mM $MgCl_2$ and [^{18}F]**AQ28A** at ~ 100 kBq/ml. Blocking experiments were performed by co-incubation with 10 µM of the PDE10A-selective inhibitor MP-10 (provided by H. Lundbeck A/S, Copenhagen, Denmark). After incubation, the sections were washed in an ice-cold TRIS buffer (50 mM; pH 7.4/4°C) for 2 × 2 min and ice-cold deionized water for 1 × 5 sec, dried in a stream of cold air and exposed to phosphor imaging plates for about 90 min. The plates were scanned and digitized using a HD-CR 35 Bio high resolution scanner (raytest Isotopenmessgeräte GmbH, Straubenhardt, Germany) and the images were analyzed using the Aida software (AIDA Image Analyzer; raytest Isotopenmessgeräte GmbH, Straubenhardt, Germany).

Animal PET/MR studies

All PET/MRI scans were performed using a preclinical PET/MRI system (nanoScan®, Mediso Medical Imaging Systems, Budapest, Hungary). Female CD1 mice (n= 3 baseline, n=2 blocking; 10-12 weeks, 31.0 ± 3.6 g) were housed overnight at 24°C in an incubator (HPP110 life, Memmert GmbH & Co. KG, Schwabach, Germany). For blocking experiments the mice received intraperitoneal (i.p.) injections of MP-10 (5 mg/kg; dissolved in 10% DMSO in 0.9% saline) 30 min prior to the PET start. The animals were anaesthetized (Anaesthesia Unit U-410, agntho's, Lidingö, Sweden) 25 minutes later with isoflurane (1.8%, 0.35 L/min) delivered in a 60% oxygen/40% air mixture (Gas Blender 100 Series, MCQ instruments, Rome, Italy) and their body temperature maintained at 37°C with a thermal bed system. [^{18}F]**AQ28A** was administered as a bolus intravenous (i.v.) injection of 9.7 ± 2.4 MBq via the lateral tail vein, and a dynamic 60 minute PET scan was started. The list-mode data were reconstructed into 23 frames (15×1 minutes, 8x5 minutes) with 3D-ordered subset expectation maximization (OSEM), 4 iterations and 6 subsets using an energy window of 400-600 keV, coincidence mode of 1-5. After the PET scan, a MRI scan was performed for anatomical orientation and attenuation correction on a 1T magnet using a T1-weighted gradient echo

sequence (TR=15 ms, TE=2.6 ms). The data analysis was done with PMOD (PMOD Technologies Ltd, Zurich, Switzerland, v. 3.601) and an atlas-based method was used to obtain SUV time-activity curves for the striatum, cerebellum and the whole brain.

In vivo metabolism of [^{18}F]AQ28A

[^{18}F]**AQ28A** (50-60 MBq in 150 µL isotonic saline, 96.9 ± 34.9 GBq/µmol) was injected via a tail vein in female CD1 mice (10-12 weeks, 20-25 g, n=3). At 30 min p.i., retro-orbital whole blood sampling was used in briefly anaesthetized mice (70% CO_2/30%O_2) by penetrating the retro-orbital sinus with a heparinized Pasteur pipette immediately before cervical dislocation and excision of brains (n=3).

Plasma samples were obtained by centrifugation of the blood at 15,000 *g* at 4°C for 2 min. The brains were excised and homogenized in TRIS buffer (50 mM; pH 7.4/4°C) on ice and a Glass/PTFE Potter Elvehjem tissue grinder (Potter S, B. Braun Biotech International, Sartorius AG, Göttingen, Germany).

Protein precipitation of plasma and brain samples was performed in triplicate with ice-cold MeCN:H_2O 8:2 (v/v) (sample:solvent 1:4 v/v). The samples were vortexed (1 min), incubated on ice (10 min) and centrifuged at 12,000□ *g* (5 min). Supernatants were collected, and MeCN:H_2O 8:2 (v/v) was added to the precipitates to repeat the extraction. Aliquots of the supernatants as well as the precipitates were measured using a gamma counter. Extraction efficacies were calculated as the ratio of radioactivity in the supernatant by the total radioactivity in the sample (precipitate + supernatant). Combined supernatants of each sample were concentrated under a nitrogen stream at 70°C and analyzed by radio-HPLC (system **C**). The peak corresponding to the radiotracer was identified by the overlap of the HPLC profile of the reference compound obtained under the same HPLC conditions as for the radiometabolite analyses (system **C**). In two additional female CD1 mice the cerebellum was separated from the remaining brain and the samples were processed and analyzed as described above.

Ex vivo autoradiography

For analysis of the distribution of [^{18}F]**AQ28A** in brain *in vivo*, the tracer was administered intravenously into a single female CD1 mouse (~ 60 MBq in 150 µL isotonic saline). The brain was isolated at 30 min p.i., after brief anesthesia (70% CO_2/30%O_2) and cervical dislocation, immediately frozen in isopentane at -30°C. Cryosections were obtained (12 µm; Microm HM 560; Thermo Fisher Scientific Inc., Walldorf, Germany), mounted on microscope slides, dried at room temperature, and exposed to phosphor imaging plates for about 60 min. The plates were scanned and digitized using a HD-CR-35 Bio high resolution scanner (raytest

Isotopenmessgeräte GmbH, Straubenhardt, Germany) and the images were analyzed using the Aida software (AIDA Image Analyzer; raytest Isotopenmessgeräte GmbH, Straubenhardt, Germany).

Results and discussion

Out of our series of fluorinated PDE10A inhibitors bearing a 2-fluoropyridinyl moiety,[38] **AQ28A** (Scheme 1) was selected for ^{18}F-radiolabeling because of the high inhibitory potency towards PDE10A and the high selectivity towards all other PDE isoforms. We introduced the fluorine at an aromatic position to reduce the formation of brain penetrant radiometabolites, which has been observed for PDE radioligands labeled *via* a ^{18}F-alkyl chain.[26, 41]

Chemistry

The bromo precursor **AQ46** and the nitro precursor **AQ63** for radiofluorination were synthesized as depicted in Scheme 1. At first, a bromo leaving group was chosen for heteroaromatic radiofluorination according to the literature.[42-44]

Organic synthesis and radiolabeling of the bromo precursor

Starting from the commercially available 6-bromopyridin-3-ylboronic acid **2** with **1**[38] (Scheme 1) the bromo precursor **AQ46** was obtained by a palladium-catalyzed Suzuki-Miyaura reaction in 16% yield. As side reaction, the substitution of the second bromine (position 8) in **AQ46** was observed to some extent reducing the overall reaction yield. The high reactivity of bromine in the *ortho*-position of the pyridine ring (position 6') in **AQ46** can also lead to undesired couplings.[45, 46] Therefore it would be advantageous to design a precursor molecule containing an unreactive group in terms of cross-coupling at that position. Thus, possessing the bromo precursor **AQ46** we explored the aromatic bromo-to-fluoro nucleophilic substitution, and performed preliminary *in vitro* characterization of [^{18}F]**AQ28A**.

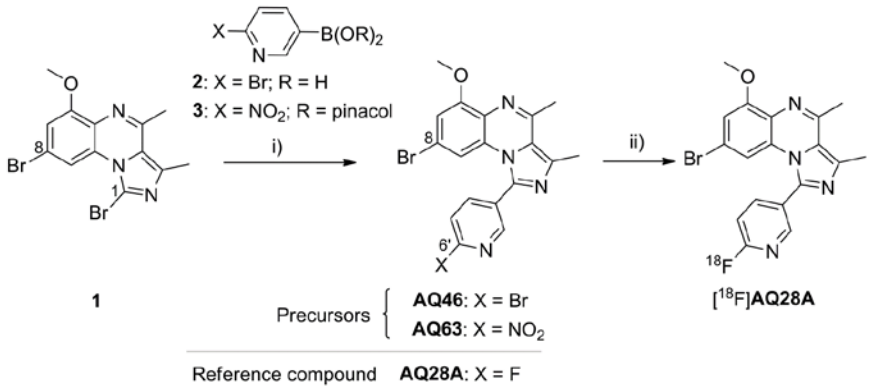

Scheme 1. Structure of reference compound **AQ28A** and preparation of precursors **AQ46** and **AQ63** by Suzuki couplings followed by ^{18}F-labeling; Reactants and conditions: i) $Pd(PPh_3)_4$, K_2CO_3, 1,4-dioxane/H_2O, reflux, 18-23 h; ii) $K_{2.2.2}$, K_2CO_3,[^{18}F]F^-, DMSO, temperature, reaction time

Manual radiolabeling of the bromo precursor AQ46 was performed in DMSO varying the amount of precursor, reaction time and temperature. The optimal bromo-to-fluoro exchange was achieved with 1 mg of AQ46 at 140°C affording [^{18}F]AQ28A after 10 min with labeling efficiencies of ~38% (Figure 2). Slightly higher labeling efficiencies (42% after 10 min) were obtained with 2 mg precursor, while lowering temperature decreased the efficiency (7% after 10 min at 120°C). We observed a decrease in radiolabeling efficiencies also at increasing reaction times in accordance with reports on decomposition of radiolabeled products obtained by bromo-to-fluoro exchanges at the pyridine system (Figure 2A). In summary, suitable labeling results with labeling efficiencies of about 38% were obtained using 1 mg of the bromo precursor AQ46 in DMSO at 140°C for 10 min.

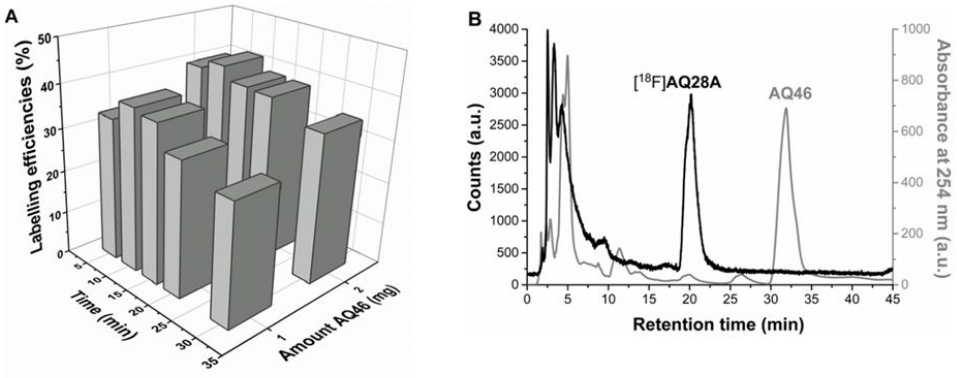

Figure 2. A) Labeling efficiencies of [^{18}F]**AQ28A** in function of the time and amount of precursor in DMSO at 140°C; and B) HPLC profile of semi-preparative separation of [^{18}F]**AQ28A** from the bromo precursor **AQ46** using system **A** (column: Multosphere 120 RP 18-AQ, eluent: MeCN/20 mM aqueous ammonium formiate 40/60 (v/v), flow: 3 mL/min) [a.u. – arbitrary units]

[^{18}F]**AQ28A** was isolated from the reaction mixture by a semi-preparative HPLC (system **A**, Figure 2B) and SPE. After formulation in 0.9% saline solution containing 10% ethanol, [^{18}F]**AQ28A** was obtained with a radiochemical yield of 10-12 % (n = 2), a radiochemical purity of ≥ 95%, and specific activities of 38-47 GBq.µmol^{-1} (n = 2, EOS). Noteworthy, the amount of [^{18}F]**AQ28A** obtained by this procedure was not sufficient for extensive investigation of

metabolism and pharmacokinetics *in vivo*, and we decided to develop an alternative precursor for heteroaromatic radiofluorination.

Organic synthesis and radiolabeling of the nitro precursor

The nitro group is reported to be a better leaving group than bromine in nucleophilic aromatic substitutions with [^{18}F]fluoride.[44] Accordingly we synthesized a nitro precursor in two steps starting from the 2-nitro-5-bromopyridine **4** (Scheme 2). Miyaura borylation reaction of **4** with bis(pinacolato)diboron **5** gave the pinacol boronic ester **3** in 74% yield.[47] The precursor **AQ63** was obtained by subsequent Suzuki coupling of **3** with imidazo[1,5-*a*]quinoxaline **1** in 29% yield (Scheme 1). The achieved yield of the nitro precursor **AQ63** was twice as high as that of the bromo precursor **AQ46**, despite similar reaction rates (~ 30% of **1** was recovered in both reactions). Most likely, the higher yield might be caused by the unreactive nitro group at the *ortho*-position (position 6') of the pyridine, thus hindering an additional Suzuki reaction at this position.

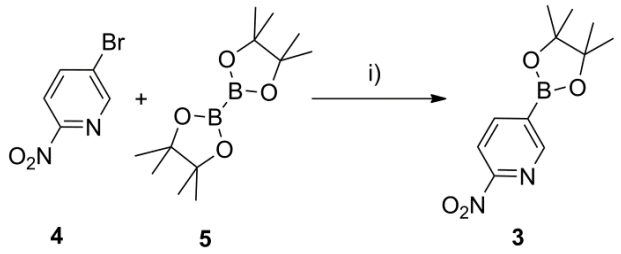

4 **5** **3**

Scheme 2. Miyaura borylation of **4** to give pinacol boronic ester **3**; reactants and conditions: i) Pd(dppf)Cl_2, KOAc, 1,4-dioxane, reflux, 1 h

We optimized manual radiolabeling of **AQ63** with a constant amount of 1 mg precursor and systematically evaluated the impact of reaction parameters such as solvent, reaction time, temperature, as well as conventional and microwave activation on labeling efficiencies. Considerably lower labeling efficiencies (≤ 40%) were obtained by using MeCN (80°C) and DMF (140°C) (Figure 3), while much higher labeling efficiencies of about 76% were achieved in DMSO at 120°C after 5 min. Although by microwave activation slightly higher labelling efficiencies (84%) were obtained in a shorter reaction time (75W, 120°C, 1 min, DMSO), we decided to transfer the thermal heating approach to an automated synthesis module because currently no microwave device-coupled synthesis module is commercially available.

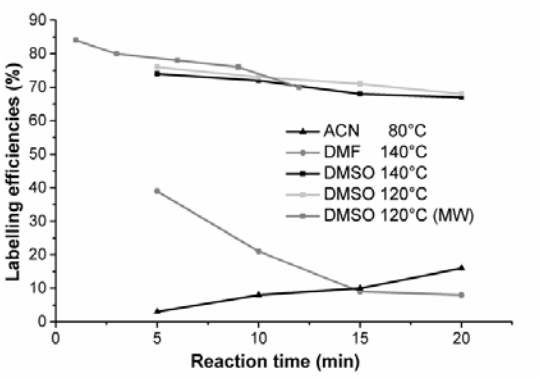

Figure 3. Labeling efficiencies depending on solvent, reaction time, temperature and activation mode using the nitro precursor **AQ63** (MW=microwave heating)

Automated radiosynthesis of [^{18}F]AQ28A

The automated radiosynthesis of [^{18}F]**AQ28A** was carried out using the synthesis module TRACERlab™ FX F-N. According to the previous optimization, nucleophilic substitution of the nitro precursor **AQ63** was performed using the K[^{18}F]F-$K_{2.2.2}$-carbonate complex in DMSO at 120°C for 8 min with starting activities of 2-15 GBq [^{18}F]F^-, and [^{18}F]**AQ28A** was obtained with labeling efficiencies of 62 □ 8% (n=3). [^{18}F]**AQ28A** was isolated by semi-preparative HPLC (Figure 4A; for **AQ63** t_R□ 45 min), purified by SPE and formulated in sterile 0.9% saline solution containing 10% EtOH. [^{18}F]**AQ28A** was reproducibly obtained within 70-80 min synthesis time with radiochemical yields of 33 ± 6% (n = 3), high radiochemical purities of ≥ 97% and with specific activities of 96-145 GBq μmol^{-1} (n = 3, EOS). Co-injection of the corresponding reference compound **AQ28A** confirmed the identity of [^{18}F]**AQ28A** by analytical HPLC (Figure 4B).

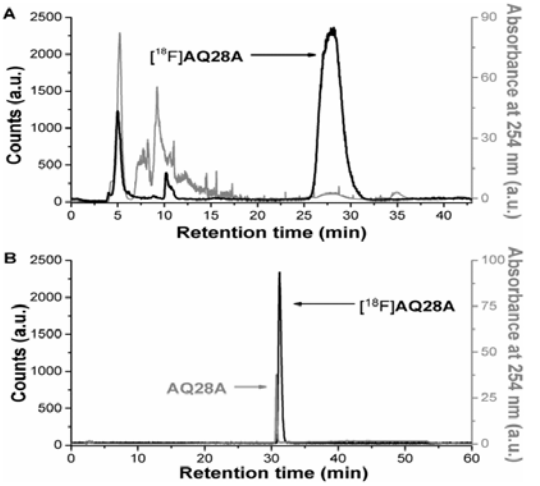

Figure 4. HPLC profiles of (A) semi-preparative separation of [^{18}F]**AQ28A** using system B (column: Reprosil-Pur C18-AQ, eluent: MeCN/H_2O/TFA 30/70/0.05 (v/v/v), flow: 3 mL/min) and

(B) analytical HPLC of [^{18}F]**AQ28A** spiked with reference compound **AQ28A**, system C (column: Reprosil-Pur C18-AQ, eluent: 10-80% (10-40 min) MeCN in 20 mM aq. NH_4OAc, flow: 1 mL/min) [a.u. – arbitrary units]

Physicochemical properties of [^{18}F]AQ28A

[^{18}F]**AQ28A** was stable (radiochemical purity ≥98%) in PBS, Tris-HCl buffer systems, and pig plasma at 37°C for 60 min as well as in formulation for up to 3 hours. The lipophilicity of [^{18}F]**AQ28A** in terms of log*D* was estimated by the shake-flask method in two *n*-octanol/buffer systems (PBS = log$D_{7.4}$; Tris-HCl = log$D_{7.2}$). In both systems, similar log*D* values of 1.94 ± 0.44 and 1.96 ± 0.30 were estimated, which correspond with the values determined for successfully applied PET radiotracers for brain imaging.[48, 49]

***In vitro* and *in vivo* characterization**

Affinity determination

The affinity of [^{18}F]**AQ28A** for rat striatal PDE10A has been determined *in vitro* by a homologous competitive binding experiment with a K_D value of 4.3 nM, which corresponds with the previously determined inhibitory potency of **AQ28A** (IC_{50} value =2.95 nM).[38]

Autoradiography *in vitro*

The distribution of binding sites of [^{18}F]**AQ28A** in brain was analyzed by in vitro autoradiography. Although brain slices of young adult mice and rats and juvenile pigs were used for that purpose, we do not expect significant age-related variations because changes in PDE10A expression were reported only in rodents of much higher difference in age.[50] In mouse brain, a high accumulation of [^{18}F]**AQ28A** was observed in PDE10A-rich regions like the striatum, the striatofugal projections and the olfactory tubercle (Figure 5A). Corresponding to this and to the expression of PDE10A described in various mammalian species,[4, 5] a high accumulation of [^{18}F]**AQ28A** was also found in the striata of rat and pig and in the olfactory tubercle of rat brain (Figure 5D, 5G). Target specificity of [^{18}F]**AQ28A** was further proven by the significantly reduced binding in the presence of 10 µM of the specific inhibitor MP-10 (Figure 5B, 5E, and 5H). Thus, [^{18}F]**AQ28A** compares favorably with our previously developed radioligand [^{18}F]**IV**,[36] which was not displaced by MP-10, probably due to off-target binding to PDE3A.

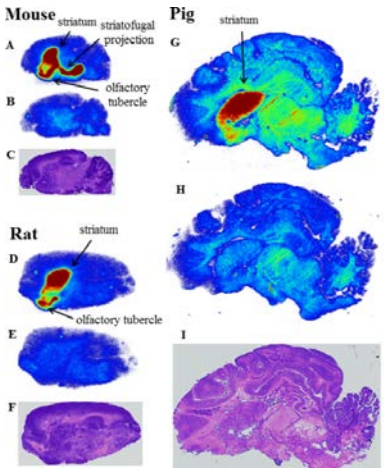

Figure 5. *In vitro* autoradiography studies on sagittal mouse, rat and pig brain slices. Total binding of [^{18}F]**AQ28A** (A, D and G), non-specific binding in the presence of 10 µM MP-10 (B, E and H) and Nissl-stained slices after autoradiography (C, F and I) for the identification of brain regions; differences in PDE10A distribution are caused by different section planes

***In vivo* PET/MR studies**

Animal PET/MR studies were performed in female CD1 mice after i.v. injection of [^{18}F]**AQ28A**. Under baseline condition, the radioactivity uptake in striatum, cerebellum, and whole brain reached peak values of SUV = 2.7, 2.3, and 1.8, respectively (mean; n=3) (Figure 6; 7A). For [^{18}F]**JNJ41510417** and for [^{18}F]**JNJ41510152** a SUV in rats of ~0.6 and ~1.4 was described.[26] According to the expression pattern of PDE10A,[51] the washout of radioactivity from cerebellum, was faster than from striatum. This resulted in striatum-to-cerebellum ratios of initially >1.4, which remained at a relatively stable level of >1 after 20 min p.i..

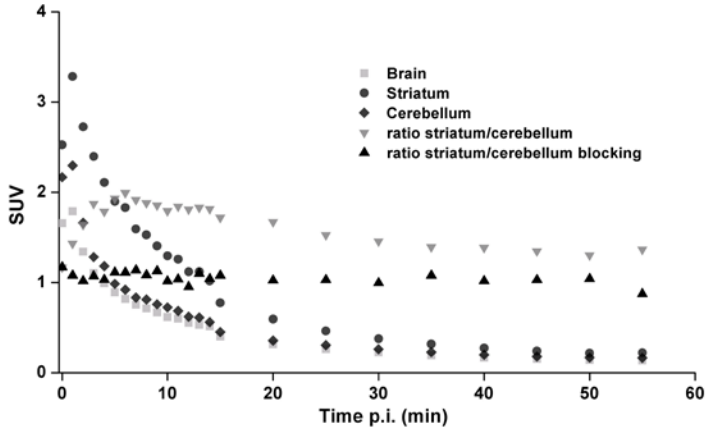

Figure 6. Time-activity curves for whole brain, striatum and cerebellum under baseline condition, and the ratios striatum/cerebellum under baseline and blocking conditions (mean values; n=3,

female CD1 mouse) of **[^{18}F]AQ28A.** The list-mode data were iteratively (OSEM, 4 iterations and 6 subsets) reconstructed into different time frames (15 × 1 min, 8 × 5min)

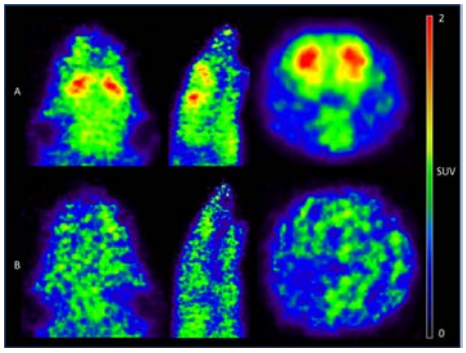

Figure 7. Representative summed PET images of **[^{18}F]AQ28A** (0 to 15 min p.i.) in coronal, sagittal and transversal view of the brain of a female CD1 mouse (age: 12 weeks). The images were acquired under (A) baseline condition showing high tracer uptake in striatum and (B) pre-blocking condition using MP-10 (5 mg/kg, i.p., 30 min prior to the injection of **[^{18}F]AQ28A**)

PET scans performed under blocking conditions by administration of 5 mg/kg MP-10 at 30 min prior to the radioligand revealed a significantly reduced uptake of radioactivity in the striatum in comparison to the baseline scan (~60%; Figure 7) and a reduction of specific binding as indicated by the striatum-to-cerebellum ratio (Figure 6). Furthermore, the uniform brain uptake (Figure 7B) supports the specific binding of [^{18}F]**AQ28A** to PDE10A *in vivo*.

***In vivo* metabolism of [^{18}F]AQ28A**

The *in vivo* metabolism of [^{18}F]**AQ28A** was investigated in female CD1 mice by analysis of plasma and brain samples obtained at 30 min p.i.. Extraction efficiencies of 88 ± 4% and 97 ± 2% were obtained, respectively. Aliquots of supernatants were further analyzed by radio-HPLC (Figure 8).

In plasma, [^{18}F]**AQ28A** accounted for 36 ± 3% (t_R = 31.0 min, n = 3) of the extraction fraction (Figure 8, bottom), which is comparable to the amount of intact radioligand found for [^{18}F]JNJ42259152 (54%, rats),[26] [^{18}F]AMG580 (~30%, baboons/rhesus monkeys)[33] and [^{18}F]MNI659 (~40%, humans).[29] Due to species-dependent differences, we hypothesize that higher amounts of intact [^{18}F]**AQ28A** will be detected in non-rodent species.[52, 53] All radiometabolites of [^{18}F]**AQ28A** were more hydrophilic than the parent compound according to their retention times. One major radiometabolite was found, [^{18}F]**M1** (t_R = 27.0 min, 28-38%), probably resulting from hydroxylation or *O*-demethylation of [^{18}F]**AQ28A**.[37]

In whole brain extracts intact [^{18}F]**AQ28A** revealed 71 ± 8% (n = 3) of total radioactivity at 30 min p.i. (Figure 8, middle). Two radiometabolites which were also detected in plasma account for about 30% of total radioactivity in brain. Although this rather high value makes penetration of the blood-brain barrier more likely than contamination during the workup of the samples, interference with the quantification of the radiotracer cannot be ruled out.[49, 54] Because we detected no significant differences regarding the fraction of intact [^{18}F]**AQ28A** in cerebellum (63 ± 6%, Figure 8, top) and cerebrum (65 ± 4%), the radiometabolites in brain contribute probably uniformly to the time-activity curves. Furthermore, in the case of [^{18}F]**JNJ42259152** kinetic modelling in rats[26] and in first clinical trials[28] provided reliable BP_{ND} quantification even when radiometabolites were present in the brain.

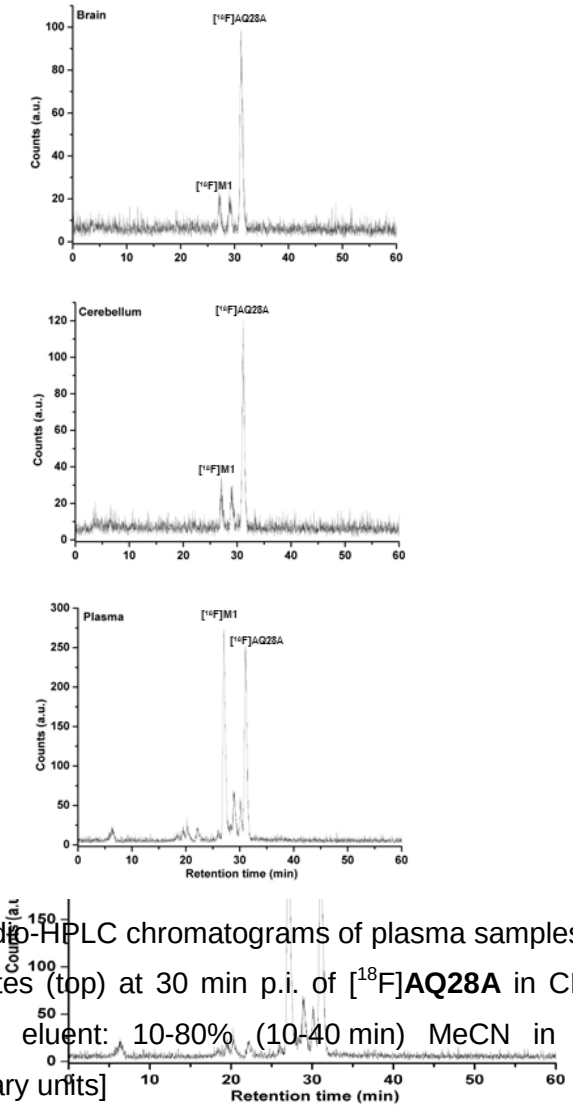

Figure 8. Analytical radio-HPLC chromatograms of plasma samples (bottom), brain (middle) and cerebellum homogenates (top) at 30 min p.i. of [^{18}F]**AQ28A** in CD1 mice, system **C** (column: Reprosil-Pur C18-AQ, eluent: 10-80% (10-40 min) MeCN in 20 mM aq. NH_4OAc, flow: 1 mL/min). [a.u.- arbitrary units]

Ex vivo autoradiographic study

The distribution pattern of [^{18}F]**AQ28A** in CD1 mouse brain was investigated by *ex vivo* autoradiography of sagittal brain slices obtained at 30 min p.i. The highest accumulation of radioactivity was detected in the striatum and the olfactory tubercle (Figure 9), referred to as PDE10A-rich regions.[4, 5] All other brain regions showed significantly lower accumulation of [^{18}F]**AQ28A**. Thus, the distribution pattern of [^{18}F]**AQ28A** in the *ex vivo* autoradiography matches the distribution found in the *in vitro* autoradiography studies and indicates the potential of [^{18}F]**AQ28A** to visualize PDE10A *in vivo*.

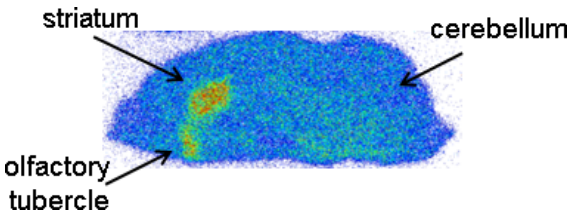

Figure 9. *Ex vivo* autoradiographic image of sagittal mouse brain slice 30 min p.i. of [^{18}F]**AQ28A**

Although the radiometabolites detected in mouse brain might result in a higher non-specific binding *ex vivo* compared to *in vitro*, they obviously do not effect off-target accumulation of radioactivity in brain.

Conclusion

For radiosynthesis of [^{18}F]**AQ28A** the nitro precursor **AQ63** is superior to the bromo precursor **AQ46** considering the yields of precursor obtained in the Suzuki reaction as well as because of significantly improved radiolabeling efficiencies. Starting from the nitro precursor **AQ63**, a fully automated radiosynthesis of [^{18}F]**AQ28A** was achieved, delivering the product in good radiochemical yields and high radiochemical purities. *In vitro* autoradiography demonstrated the suitability of [^{18}F]**AQ28A** as a specific radioligand to visualize the PDE10A protein in different species. Furthermore, the brain kinetics investigated by animal PET revealed a specific accumulation of [^{18}F]**AQ28A** in the PDE10A-rich striatum, along with a lack of specific accumulation after blocking PDE10A with MP-10. Altogether, the data make [^{18}F]**AQ28A** a promising candidate for imaging of PDE10A in rodents by PET.

Acknowledgments

We thank Dr. Karsten Franke (HZDR) for the production of [^{18}F]fluoride, Tina Spalholz (HZDR) for performing the shake-flask experiments, and Dr. Lothar Hennig (Leipzig University) for measuring NMR spectra.

References

[1] S. H. Francis, M. A. Blount and J. D. Corbin, *Physiol. Rev.*, **2011**, *91*, 651.
[2] K. Fujishige, J. Kotera, H. Michibata, K. Yuasa, S. Takebayashi, K. Okumura and K. Omori, *J. Biol. Chem.*, **1999**, *274*, 18438.
[3] K. Fujishige, J. Kotera and K. Omori, *Eur. J. Biochem.*, **1999**, *266*, 1118.
[4] T. F. Seeger, B. Bartlett, T. M. Coskran, J. S. Culp, L. C. James, D. L. Krull, J. Lanfear, A. M. Ryan, C. J. Schmidt, C. A. Strick, A. H. Varghese, R. D. Williams, P. G. Wylie and F. S. Menniti, *Brain Res.*, **2003**, *985*, 113.
[5] T. M. Coskran, D. Morton, F. S. Menniti, W. O. Adamowicz, R. J. Kleiman, A. M. Ryan, C. A. Strick, C. J. Schmidt and D. T. Stephenson, *J. Histochem. Cytochem.*, **2006**, *54*, 1205.
[6] A. Charara, M. Sidibé and Y. Smith, *Contemporary clinical neurology: surgical treatment of parkinson's disease and other movement disorders*, (Eds: D. Tarsy, J. L. Vitek and A. M. Lozano), Humana Press Inc., Totowa, **2003**, pp. 19.
[7] A. K. Afifi, *Semin. Pediatr. Neurol.*, **2003**, *10*, 3.
[8] C. Gerfen, T. Engber, L. Mahan, Z. Susel, T. Chase, F. Monsma and D. Sibley, *Science*, **1990**, *250*, 1429.
[9] J. M. Beaulieu and R. R. Gainetdinov, *Pharmacol. Rev.*, **2011**, *63*, 182.
[10] Z. Xie, W. O. Adamowicz, W. D. Eldred, A. B. Jakowski, R. J. Kleiman, D. G. Morton, D. T. Stephenson, C. A. Strick, R. D. Williams and F. S. Menniti, *Neuroscience*, **2006**, *139*, 597.
[11] S. M. Grauer, V. L. Pulito, R. L. Navarra, M. P. Kelly, C. Kelley, R. Graf, B. Langen, S. Logue, J. Brennan, L. Jiang, E. Charych, U. Egerland, F. Liu, K. L. Marquis, M. Malamas, T. Hage, T. A. Comery and N. J. Brandon, *J. Pharmacol. Exper.Ther.*, **2009**, *331*, 574.
[12] C. J. Schmidt, D. S. Chapin, J. Cianfrogna, M. L. Corman, M. Hajos, J. F. Harms, W. E. Hoffman, L. A. Lebel, S. A. McCarthy, F. R. Nelson, C. Proulx-LaFrance, M. J. Majchrzak, A. D. Ramirez, K. Schmidt, P. A. Seymour, J. A. Siuciak, F. D. Tingley, R. D. Williams, P. R. Verhoest and F. S. Menniti, *J. Pharmacol. Exper. Ther.*, **2008**, *325*, 681.
[13] J. A. Siuciak, D. S. Chapin, J. F. Harms, L. A. Lebel, S. A. McCarthy, L. Chambers, A. Shrikhande, S. Wong, F. S. Menniti and C. J. Schmidt, *Neuropharmacology*, **2006**, *51*, 386.
[14] J. B. Tuttle and B. L. Kormos, *Small Molecule Therapeutics for Schizophrenia*, (Eds: S. Celanire and S. Poli), Springer International Publishing, **2015**, pp. 255.
[15] J. Kehler and J. Nielsen, *Curr. Pharm. Des.* , **2011**, *17*, 137.
[16] C. Giampà, D. Laurenti, S. Anzilotti, G. Bernardi, F. S. Menniti and F. R. Fusco, *Plos ONE*, **2010**, *5*, 13417.
[17] C. Giampà, S. Patassini, A. Borreca, D. Laurenti, F. Marullo, G. Bernardi, F. S. Menniti and F. R. Fusco, *Neurobiol. Dis.*, **2009**, *34*, 450.
[18] Takeda, *An [^{11}C]T-773 Positron Emission Tomography (PET) Study to Determine Phosphodiesterase10A Occupancy by TAK-063*, **2014**, Accessed 30.07.2015, https://ClinicalTrials.gov/show/NCT02370602.
[19] *Hoffmann-La Roche, A PET Study With RO5545965 in Healthy Male Volunteers*, **2013**, Accessed 24.04.2016, https://ClinicalTrials.gov/show/NCT01923025.
[20] *Chdi Foundation Inc, Imaging of PDE10A Enzyme Levels in Huntington's Disease Gene Expansion Carriers and Healthy Controls With PET*, **2014**, Accessed 25.04.2016, https://ClinicalTrials.gov/show/NCT02061722.

[21] D. S. Russell, O. Barret, D. L. Jennings, J. H. Friedman, G. D. Tamagnan, D. Thomae, D. Alagille, T. J. Morley, C. Papin, S. Papapetropoulos, R. N. Waterhouse, J. P. Seibyl and K. L. Marek, *JAMA Neurol.*, **2014**, *71*, 1520.
[22] Z. Tu, J. D. Fan, S. H. Li, L. A. Jones, J. Q. Cui, P. K. Padakanti, J. B. Xu, D. X. Zeng, K. I. Shoghi, J. S. Perlmutter and R. H. Mach, *Bioorg. Med. Chem.*, **2011**, *19*, 1666.
[23] C. Plisson, D. Weinzimmer, S. Jakobsen, S. Natesan, C. Salinas, S.-F. Lin, D. Labaree, M.-Q. Zheng, N. Nabulsi, T. R. Marques, S. Kapur, E. Kawanishi, T. Saijo, R. N. Gunn, R. E. Carson and E. A. Rabiner, *J. Nucl. Med.*, **2014**, *55*, 595.
[24] J. Kehler, J. P. Kilburn, S. Estrada, S. R. Christensen, A. Wall, A. Thibblin, M. Lubberink, C. Bundgaard, L. T. Brennum, B. Steiniger-Brach, C. T. Christoffersen, S. Timmermann, M. Kreilgaard, G. Antoni, B. Bang-Andersen and J. Nielsen, *J. Nucl. Med.*, **2014**, *55*, 1513.
[25] J. I. Andres, M. De Angelis, J. Alcazar, L. Iturrino, X. Langlois, S. Dedeurwaerdere, I. Lenaerts, G. Vanhoof, S. Celen and G. Bormans, *J. Med. Chem.*, **2011**, *54*, 5820.
[26] S. Celen, M. Koole, M. Ooms, M. De Angelis, I. Sannen, J. Cornelis, J. Alcazar, M. Schmidt, A. Verbruggen, X. Langlois, K. Van Laere, J. I. Andrés and G. Bormans, *Neuroimage*, **2013**, *82*, 13.
[27] K. Van Laere, R. U. Ahmad, H. Hudyana, K. Dubois, M. E. Schmidt, S. Celen, G. Bormans and M. Koole, *J. Nucl. Med.*, **2013**, *54*, 1285.
[28] K. Van Laere, R. Ahmad, H. Hudyana, S. Celen, K. Dubois, M. Schmidt, G. Bormans and M. Koole, *Eur. J. Nucl. Med. Mol. Imag.*, **2013**, *40*, 254.
[29] C. D. Cox, J. L. Bunda, B. A. Flores and W. Shipe, *Pyrimidinones As PDE10A Inhibitors*, **2010**, WO2010138585A1.
[30] O. Barret, D. Thomae, A. Tavares, D. Alagille, C. Papin, R. Waterhouse, T. McCarthy, D. Jennings, K. Marek, D. Russell, J. Seibyl and G. Tamagnan, *J. Nucl. Med.*, **2014**, *55*, 1297.
[31] *Forum Pharmaceuticals Inc, Study of EVP-6308 to Assess the Dose- and Concentration-dependent Displacement of [^{18}F]MNI-659 by EVP-6308*, **2013**, Accessed 25.04.2016, https://ClinicalTrials.gov/show/NCT02001389.
[32] Pfizer, *A Study To Evaluate The PDE10 Enzyme Occupancy Following A Single Dose Of PF-02545920 In Healthy Male Volunteers*, **2014**, Accessed 25.04.2016, https://ClinicalTrials.gov/show/NCT01918202.
[33] H. Chen, D. Lester-Zeiner, J. Shi, S. Miller, C. Glaus, E. Hu, N. Chen, J. Able, C. Biorn, J. Wong, J. Ma, K. Michelsen, G. Hill Della Puppa, T. Kazules, H. H. Dou, S. Talreja, X. Zhao, A. Chen, S. Rumfelt, R. K. Kunz, H. Ye, O. R. Thiel, T. Williamson, C. Davis, A. Porter, D. Immke, J. R. Allen and J. Treanor, *J. Pharmacol. Exp. Therap.*, **2015**, *352*, 327.
[34] D.-R. Hwang, E. Hu, J. R. Allen, C. Davis, J. Treanor, S. Miller, H. Chen, B. Shi, T. K. Narayanan, O. Barret, D. Alagille, Z. Yu and M. Slifstein, *Nucl. Med. Biol.*, **2015**, *42*, 654.
[35] G. Schwan, G. Barbar Asskar, N. Höfgen, L. Kubicova, U. Funke, U. Egerland, M. Zahn, K. Nieber, M. Scheunemann, N. Sträter, P. Brust and D. Briel, *ChemMedChem*, **2014**, *9*, 1476.
[36] U. Funke, W. Deuther-Conrad, G. Schwan, A. Maisonial, M. Scheunemann, S. Fischer, A. Hiller, D. Briel and P. Brust, *Pharmaceuticals*, **2012**, *5*, 169.
[37] M. S. Malamas, Y. Ni, J. Erdei, H. Stange, R. Schindler, H.-J. Lankau, C. Grunwald, K. Y. Fan, K. Parris, B. Langen, U. Egerland, T. Hage, K. L. Marquis, S. Grauer, J. Brennan, R. Navarra, R. Graf, B. L. Harrison, A. Robichaud, T. Kronbach, M. N. Pangalos, N. Hoefgen and N. J. Brandon, *J. Med. Chem.*, **2011**, *54*, 7621.
[38] S. Wagner, M. Scheunemann, K. Dipper, U. Egerland, N. Hoefgen, J. Steinbach and P. Brust, *Eur. J. Med. Chem.*, **2016**, *107*, 97.
[39] F. Dolle, *Curr. Pharmac. Des.*, **2005**, *11*, 3221.
[40] Y. Cheng and W. H. Prusoff, *Biochem. Pharmacol.*, **1973**, *22*, 3099.

[41] S. Schröder, B. Wenzel, W. Deuther-Conrad, R. Teodoro, U. Egerland, M. Kranz, M. Scheunemann, N. Höfgen, J. Steinbach and P. Brust, *Molecules*, **2015**, *20*, 9591.
[42] M. Karramkam, F. Hinnen, M. Berrehouma, C. Hlavacek, F. Vaufrey, C. Halldin, J. A. McCarron, V. W. Pike and F. Dollé, *Bioorg. Med. Chem.*, **2003**, *11*, 2769.
[43] A. Horti, H. T. Ravert, E. D. London and R. F. Dannals, *J. Labelled Comp. Radiopharm.*, **1996**, *38*, 355.
[44] L. Dolci, F. Dolle, H. Valette, F. Vaufrey, C. Fuseau, M. Bottlaender and C. Crouzel, *Bioorg. Med. Chem.*, **1999**, *7*, 467.
[45] A. S. Voisin-Chiret, A. Bouillon, G. Burzicki, M. Célant, R. Legay, H. El-Kashef and S. Rault, *Tetrahedron*, **2009**, *65*, 607.
[46] S. Perato, A. S. Voisin-Chiret, J. Sopková-de Oliveira Santos, R. Legay, H. Oulyadi and S. Rault, *Tetrahedron*, **2012**, *68*, 1910.
[47] T. Ishiyama, M. Murata and N. Miyaura, *J. Org. Chem.*, **1995**, *60*, 7508.
[48] R. N. Waterhouse, *Mol. Imag. Biol.*, **2003**, *5*, 376.
[49] V. W. Pike, *Trends Pharmacol. Sci.*, **2009**, *30*, 431.
[50] M. P. Kelly, W. Adamowicz, S. Bove, A. J. Hartman, A. Mariga, G. Pathak, V. Reinhart, A. Romegialli and R. J. Kleiman, *Cell Signal*, **2014**, *26*, 383.
[51] M. Ooms, S. Celen, M. Koole, X. Langlois, M. Schmidt, M. De Angelis, J. I. Andres, A. Verbruggen, K. Van Laere and G. Bormans, *Nucl. Med. Biol.*, **2014**, *41*, 695.
[52] M. Schou, S. S. Zoghbi, H. U. Shetty, E. Shchukin, J. S. Liow, J. Hong, B. A. Andree, B. Gulyas, L. Farde, R. B. Innis, V. W. Pike and C. Halldin, *Mol. Imag. Biol.*, **2009**, *11*, 23.
[53] G. C. Van de Bittner, E. L. Ricq and J. M. Hooker, *Acc. Chem. Res.*, **2014**, *47*, 3127.
[54] S. S. Zoghbi, H. U. Shetty, M. Ichise, M. Fujita, M. Imaizumi, J. S. Liow, J. Shah, J. L. Musachio, V. W. Pike and R. B. Innis, *J. Nucl. Med.*, **2006**, *47*, 520.